International Journal of Mass Spectrometry 377 (2015) 228–234

International Journal of Mass Spectrometry

journal homepage: www.elsevier.com/locate/ijms

Soft-landing electrospray ion beam deposition of sensitive oligoynes on surfaces in vacuum

Gordon Rinke[a], Stephan Rauschenbach[a,*], Stephen Schrettl[b], Tobias N. Hoheisel[b], Jonathan Blohm[a,1], Rico Gutzler[a], Federico Rosei[c], Holger Frauenrath[b], Klaus Kern[a,d]

[a] Max-Planck-Institute for Solid State Research, Nanoscale Science Department, Stuttgart, Germany
[b] Ecole Polytechnique Fédérale de Lausanne, Institute of Materials, Laboratory of Macromolecular and Organic Materials, Lausanne, Switzerland
[c] Centre for Energy, Materials and Telecommunications, Institut National de la Recherche Scientifique, Varennes, QC, Canada
[d] Institut de Physique de la Matière Condensée, Ecole Polytechnique Fédérale de Lausanne, Switzerland

ARTICLE INFO

Article history:
Received 19 March 2014
Received in revised form 6 June 2014
Accepted 27 June 2014
Available online 4 July 2014

ABSTRACT

Advances in synthetic chemistry permit the synthesis of large, highly functional, organic molecules. Characterizing the complex structure of such molecules with highly resolving, vacuum-based methods like scanning probe microscopy requires their transfer into the gas phase and further onto an atomically clean surface in ultrahigh vacuum without causing additional contamination. Conventionally this is done via sublimation in vacuum. However, similar to biological molecules, large synthetic compounds can be non-volatile and decompose upon heating. Soft-landing ion beam deposition using soft ionization methods represents an alternative approach to vacuum deposition. Using different oligoyne derivatives of the form of $R_1{-}(C{\equiv}C)_n{-}R_2$, here we demonstrate that even sensitive molecules can be handled by soft-landing electrospray ion beam deposition. We generate intact molecular ions as well as fragment ions with intact hexayne parts and deposit them on clean metal surfaces. Scanning tunneling microscopy shows that the reactive hexayne segments of the molecules of six conjugated triple bonds are intact. The molecules agglomerate into ribbon-like islands, whose internal structure can be steered by the choice of the substituents. Our results suggest the use of ion beam deposition to arrange reactive precursors for subsequent polymerization reactions.

1. Introduction

Soft ionization methods such as electrospray ionization (ESI) [1] or matrix assisted laser desorption ionization (MALDI) [2] are important methods in mass spectrometry as they allow researchers to study a broad variety of molecules with high precision. These ionization methods typically generate intact molecular gas phase ions, even of fragile biological molecules like proteins or peptides that would decompose in conventional gas phase ion sources based on electron impact or chemical ionization [3].

A less common application of soft ionization is its use as a gas phase particle source for vacuum deposition. The preparation of well-defined molecular adsorbates on atomically clean substrates for use in surface science experiments requires a well-controlled environment, such as ultrahigh vacuum (UHV, $p \approx 10^{-10}$ mbar). This environment enables the investigation of molecules with methods of highest precision, like spatial mapping of surfaces and adsorbates at atomic resolution with scanning tunneling microscopy (STM). For this purpose, however, the molecules have to be transferred to the surface as gas phase molecules, either by leaking them into vacuum or by sublimation within the UHV system. Thus the application is limited to volatile molecules, which can be evaporated without decomposition. Soft ionization sources like ESI or MALDI generate intact gas phase ions of molecules that are otherwise not accessible by conventional evaporation methods due to the fragility or high reactivity of the corresponding organic species. For ion beam deposition, the intact molecular ions are transferred from the ion source, which can be at ambient pressure, to vacuum through differentially pumped ion optics [4–7]. Although ion beam deposition is experimentally challenging, the methodology of intact deposition of molecules onto surfaces, also called ion soft-landing, can be considered as well established [8–10]. Also the deposition of molecular ions that undergo chemical

* Corresponding author. Tel.: +49 0711 689 1433; fax: +49 (0) 711 689 1662.
E-mail addresses: g.rinke@fkf.mpg.de (G. Rinke), s.rauschenbach@fkf.mpg.de (S. Rauschenbach).
[1] Present address: Department of Chemistry, University of Warwick, Coventry, United Kingdom.

http://dx.doi.org/10.1016/j.ijms.2014.06.026

reactions upon deposition, called reactive landing, is well studied mainly by chemical characterization of the surface [11–16].

In situ scanning probe microscopy investigations of surfaces after the soft-landing deposition of intact molecular ions enables the imaging of individual non-volatile molecules with submolecular resolution [17–21]. In a few examples, ordered two-dimensional [22,23] as well as three-dimensional thin film growth [23] has been observed after soft landing of intrinsically stable molecules.

Here, we extend the approach of soft-landing electrospray ion beam deposition (ES-IBD) combined with high resolution scanning tunneling microscopy to reactive molecules. We demonstrate that potentially reactive species can be brought to the surface without immediate covalent reaction. By adapting the molecular structure, we tune weak physisorption interactions responsible for the self-assembly of the molecules into ordered precursor structures, which may be covalently cross-linked in a second step by light or temperature treatment [24].

Oligoyne (OY) derivatives of the form of R–(C≡C)$_n$–R are a class of reactive organic molecules that are of interest as potential precursor molecules for the preparation of nanostructured carbon materials by a low-temperature conversion into other carbon allotropes [25–29]. Due to the high reactivity of these compounds, their synthesis and handling is challenging, in particular with an increasing number n of acetylene units [30,31]. However, the proper choice of the substituents R stabilizes oligoynes and has allowed for the preparation of molecules with up to $n = 22$ units [32]. Despite recent advances in synthesis methods, the handling and characterization by STM of OY-adlayers is limited to diacetylene molecules with $n = 2$ units. The deposition of diacetylene molecules with the Langmuir–Blodgett technique under ambient conditions yielded a self-assembled molecular network characterized by a parallel alignment of the diacetylene moiety of different molecules [33]. Other diacetelynes have been found to be thermally stable enough for sublimation onto a surface in UHV, where STM imaging evidenced the presence of the molecules and their polymerization as a result of irradiation with UV-light [34,35]. While this approach is bound to fail for longer OYs, we demonstrate here that ES-IBD can be successfully applied to the deposition of hexaynes, *i.e.* oligoyne derivatives with $n = 6$ acetylene units [36], onto atomically defined metal surfaces in UHV. For this purpose, two hexaynes with different substituents R (see Fig. 1) were used to investigate the influence of the molecular structure on deposition and subsequent self-assembly on the surface. The first one is the glycosylated hexayne (heptacosa-4′, 6′, 8′, 10′, 12′, 14′-hexynyl β-D-glucopyranoside) **1** that has a mass of 534 amu and a length of approximately 4 nm. The second one is the hexayne diester (dimethyl icosa-5,7,9,11,13,15-hexaynedioate) **2** with a mass of 346 amu and an extended length of 2.7 nm.

Initial mass spectrometry characterization shows that ESI generates intact as well as fragmented ionized species. Once an ion beam suitable for deposition is prepared, the clean metal surface in UHV is coated with the OY ion beam and subsequently characterized by STM. To avoid a strong interaction with the surface we chose the inert gold surface (Au(1 1 1)) for deposition. STM imaging at submolecular resolution shows molecular ordering at the surface for intact and even fragmented molecules with intact oligoyne segments. The self-assembly of the OYs is found to depend strongly on the substituents. The results show that very reactive molecules can be handled with ES-IBD and their self-assembly be effectively steered by optimizing the molecules shape.

2. Experimental

The investigated OY molecules with $n = 6$ acetylene units were prepared according to a synthetic protocol based on the Negishi reaction that allowed for the direct bond formation between two sp-hybridized carbon atoms [28,36]. For the ES-IBD experiment, sketched in Fig. 2, we use a home-built nano-ESI interface optimized for high ion transmission [37]. Compared to mass spectrometry, a high ion flux is crucial for an ion beam deposition experiment, because a large number of ions has to be deposited to reach a molecular coverage detectable by STM on a macroscopic surface. For instance on a typical sample surface area of 12 mm^2 approximately 2×10^{11} molecules have to be deposited for achieving a submonolayer coverage of one molecule in a typical 50 nm × 50 nm scan window.

After passing the interface, the ion beam is shaped by collisional cooling in a radio frequency (rf) ion funnel and a rf-quadrupole ion guide operated at 1 mbar and 0.02 mbar, respectively. In high vacuum another quadrupole ion guide can be used for mass selection before the beam is analyzed by time-of-flight (TOF) mass spectrometry and a retarding grid energy detector. Further, the mass spectrometry results are confirmed using an Agilent Technologies single quad mass spectrometer equipped with our home-built nano electrospray funnel-ion source [37].

In parallel to the ion beam preparation, the substrate for deposition is prepared in a separate preparation chamber under UHV conditions. A clean noble metal surface is obtained through a repeated sequence of Argon ion sputtering to remove any contamination. Subsequent annealing at high temperatures (typically 800–900 K) serves to recrystallize the surface. As a result of several sputtering/annealing cycles, a clean, atomically flat surface with atomic terraces with lateral dimensions of several 100 nm is obtained. The purity of the surface is controlled with STM before it is transferred *in situ* into the deposition chamber, which is the last chamber of the differentially pumped ES-IBD source and maintained at UHV pressure. Based on the measured beam energy, the sample is biased to adjust the collision energy. Typically, the kinetic energy of the beam is 50 eV per charge. To ensure soft-landing the sample is biased at −45 *V* resulting in a collision energy of 5 eV per charge, which is sufficiently low to avoid fragmentation upon landing [8,38,39]. The surface is then exposed to the ion beam and the deposition current is measured with an electrometer connected to the sample. The ion current integrated over time is the deposited charge, which is a measure for the delivered molecular coverage. As we can safely assume that at room temperature large, non-volatile molecules stick to a metal surface, with the knowledge of the charge state the molecular flux is precisely know in ES-IBD. Once the desired coverage is achieved the sample is again transferred *in situ* to the STM where it is imaged at room temperature or at 40 K.

For the interpretation of the STM data, a comparison with theoretical models is often helpful. Density functional theory (DFT) can provide a local electronic density of states map of a molecule, which is an important reference when analyzing the intensity on an STM image. Molecular structure optimization was carried out in the gas phase using the Orca 3.0 program with the B3LYP functional and the def2-TZVP basis set [40].

3. Mass spectrometry

A stable electrospray of negative ions for mass spectrometry and deposition of compounds **1** and **2** is achieved by dissolving them in a mixture of dichloromethane (DCM), methanol (MeOH), and chloroform ($CHCl_3$) and further dilution to a concentration of $c = 0.5 - 1.0$ mmol/L in pure MeOH.

The mass spectrum of the glycosylated hexayne **1**, displayed in Fig. 3a, shows several peaks in the range of 200–1200 Th (1 Th = 1 Thomson = 1 u/e) [41]. The most intense signal at 533 Th corresponds to the negatively charged molecule, most probably

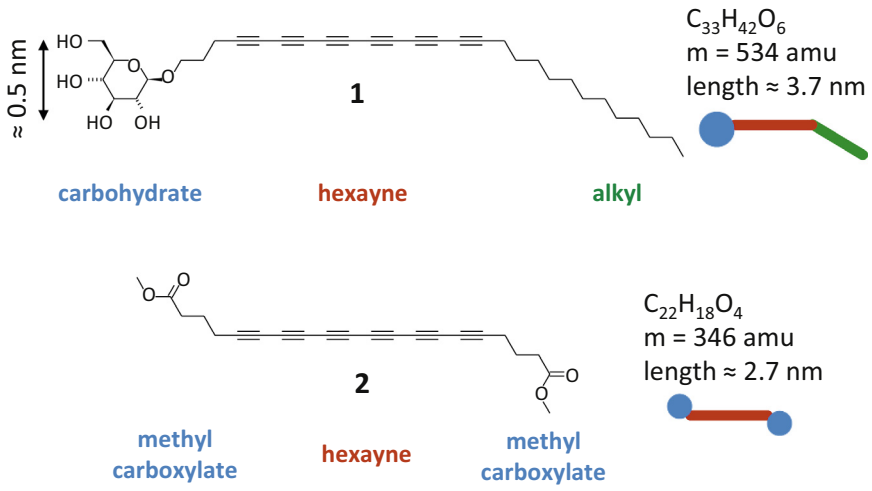

Fig. 1. Molecular structures of the used hexayne derivatives. The glycosylated hexayne **1** comprises a terminal carbohydrate group (blue) and an alkyl chain (green). The hexayne diester **2** exhibits a symmetric structure with two polar methylcarboxylate end groups (blue).

deprotonated at the carbohydrate head group. The charging can also be achieved through the addition of a Cl^-, which is present as an impurity and gives rise to the peak at 569 Th. In addition, cluster peaks are observed at 1067 and 1103 Th, corresponding to dimers, charged either by deprotonation or attachment of Cl^-. An additional group of peaks corresponding to doubly charged trimers is observed at around 800 Th. While the smaller peaks below 500 Th correspond to fragments and contaminants, the peaks with the largest intensities can be explained with the mass of the intact glycosylated hexayne **1**. It can, hence, be concluded that the sensitive hexayne triple bonds remains unaffected by the electrospray ionization procedure.

The mass spectrum of the hexayne diester **2** in Fig. 3b shows several peaks ranging from 227 to 690 Th. The peak at 345 Th corresponds to the deprotonated, intact molecule but has a relatively low intensity. Significantly higher intensities are found for the peaks at 335, 283 and 255 Th corresponding to molecules that are fragmented or have reacted, either during ionization procedure or in solution. Furthermore, peaks at 690 Th and 670 Th correspond to single negatively charged dimer of the intact molecule and to the species at 335 Th in the mass spectrum, respectively. The large fractions of fragmented/reacted molecules in the mass spectrum is possibly due to the dilution with methanol. This cannot be avoided as adding a polar solvent is needed to maintain a stable spray with sufficient intensity. Nevertheless, the mass of the fragments indicates that many of them still contain the intact hexayne segment or at least a major section of it, as may be elucidated by extracting structural information from STM after deposition on the surface (*vide infra*).

4. Deposition and STM imaging

Because the glycosylated hexayne **1** did not show a high ionization yield, an ion current of only 25 pA was detected for the transmitting the entire *m*/*z*-range. While this is enough to produce a good mass spectrum (see Fig. 3), selecting a single peak for deposition would lead to such a low current that the deposition would take extremely long, compromising the surface quality. Thus, a large

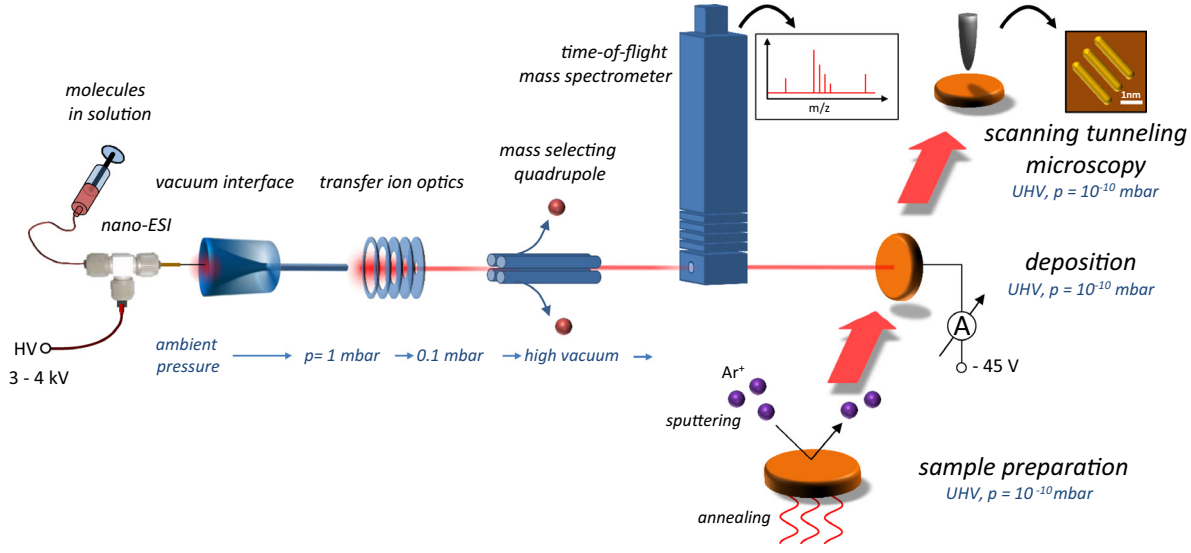

Fig. 2. Schematic illustration of the electrospray ion beam deposition setup and procedure. Ions are created by a nano-ESI interface and transferred by ion optics into UHV. A mass selecting quadrupole and a TOF mass spectrometer serve to ensure the chemical composition of the ion beam. In parallel, a metal surface is cleaned by several sputtering/annealing cycles in a separate chamber and then transferred to the deposition chamber. After deposition, the sample is transferred *in situ* to the scanning tunneling microscope.

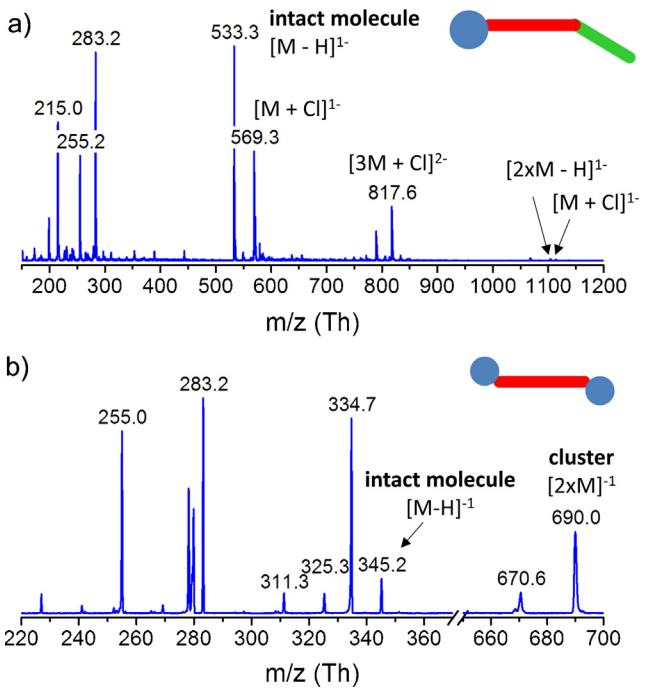

Fig. 3. (a) Mass spectra of the glycosylated hexayne **1** in negative mode show the intact molecule but also fragments and clusters. (b) Mass spectra of the hexayne diester **2** in negative mode show a low intensity of the singly charged intact molecule and more intensive fragments and clusters.

fraction of the ion beam in the *m*/*z*-window of 200–1200 Th was transmitted for a time-efficient deposition, since mass-selecting a single peak for the deposition would entail a massive ion current intensity loss. This means three types of ions are deposited on the surface: intact molecules, clusters of intact molecules and undefined fragments, with both hydrogen loss or Cl^- attachment as charging mechanism (see Fig. 3a). The information from STM imaging will be used to identify the structure of these species as well as their effect on the self-assembly.

A total charge amount of 25 pAh (pAh = pico Ampere hour) was deposited onto a freshly prepared Au(1 1 1) surface that was kept at room temperature. The sample was then imaged after *in situ* transfer into the STM chamber. At room temperature, no stable molecular agglomerations were detected by STM. However, characteristic fluctuations of the tunneling current indicated the presence of highly mobile adsorbates. Therefore, the sample needs to be cooled to 40 K for imaging, freezing out the diffusive motion of the highly mobile species.

At that temperature, large ordered islands with a brightly striped ribbon superstructure are found on the surface alongside some disordered agglomerations (Fig. 4a). The observed bright stripes of the islands exhibit a periodicity of approximately 4.6 nm. At higher magnification, the islands reveal a more detailed substructure. Each of the bright stripes consists of two rows of lobes with a periodicity of 0.5 nm positioned in a staggered arrangement (Fig. 4b). However, the bright lobes are only observed irregularly and smaller features or voids are frequently observed in their place. In between two bright rows, linear features with single kinks can be identified. Interestingly, the orientation of the kinks is pointing in opposite directions in adjacent rows.

The kinked feature is characteristic for the sp–sp^3 chain joint at an angle of approximately 140° between the hexayne and dodecyl segments of the intact molecule. The bright lobes are, hence, assigned to rows of the carbohydrate head group of **1** as the periodicity of 0.5 nm fits well to a dense packing of the latter. Along every row, the molecules alternate in orientation such that an alkyl chain (green) is always positioned next to a hexayne segment (red). This interlocked arrangement serves to accommodate the larger steric demand of the carbohydrate head group (blue) (Fig. 4b). The interpretation of the STM images is supported by DFT computations of the glycosylated hexayne **1** by calculating the conformation and electronic charge density of the molecule. The results show that the brighter section of the kinked linear features corresponds to the hexayne segments, while the darker space in between is the location of the alkyl chain (Fig. 4c).

The frequent presence of dark features of submolecular size, especially along the carbohydrate rows, is the consequence of the limited mass selection, which gives rise to the deposition of fragmented and chlorinated ion species. Judging from the STM observations, the presence of dark features does not cause distortions of the lamellar lattice structure, which excludes the incorporation of molecules fragmented under loss of the carbohydrate terminus. It is more plausible that the molecules are intact but show a lower density of states at the site of the carbohydrate. This could be explained by the presence of the chlorine ions/atoms, which were deposited as a charge carrier of some OY ions. It is known from a number of other STM studies that halogens incorporated in molecular agglomerations may appear as depressions at negative bias voltage due to their strong electronegativity [42]. Moreover, adduct charge carriers can be incorporated in lamellar structures as shown for crystalline organic salt islands, where excess Na charge carriers are incorporated [23].

The significant fraction of contaminating species co-deposited due to the wide *m*/*z*-range does not impose limitations on the self-assembly process itself. On the contrary, this supramolecular aggregation shows a great tolerance toward the incorporation of fragmented or chlorinated molecules. The arrangement of molecules on the surface suggests two distinct attractive interactions that guide the self-assembly process: dispersive interactions along the non-polar hexayne and the alkyl chains and directional hydrogen bonds between the carbohydrate groups. This type of ordering, caused by an amphiphilic binding motive can be very stable but still highly flexible, as evidenced by biological membranes or surfactant films, and has also be demonstrated to be transferable to a surface in vacuum [23].

The ion beam generated from solutions of the hexayne diester **2** contains a mixture of fragments alongside a small amount of intact molecules. This ion beam was deposited without mass selection, to explore the variety of molecular species and their self-assembly at the surface by STM. This has the advantage that fragmented ions, that had not been unambiguously identified in the mass spectrum (see Fig. 3b), can be better characterized. Samples were prepared on the Au(1 1 1) surface, onto which a charge of 25 pAh was deposited and subsequently imaged at low temperatures (40 K).

Ribbon-like islands were observed on the surface, growing from the elbow sites along the directions of the herringbone reconstruction (Fig. 5a) [43]. Each island consists of an even number of ribbons with an approximate width of 2.3 nm. Magnified images show that these islands appear to consist of rod-like elements of different contrasts. One type of island (Fig. 5b) features an almost flat topography, while the other type exhibits a stripe-like chain of lobes along the ribbon marked with arrows in Fig. 5c. In addition, islands exhibiting both types of contrasts were observed as well, suggesting that the islands consist of individual molecules held together by non-covalent interaction. For both types of islands, however, the ribbon substructure elements have a common width of 2.3 nm. Together with their asymmetric shape, this indicates that they do not correspond to the intact molecule **2** that is symmetric and has an approximated end-to-end distance of 2.7 nm. Instead, the structures observed by STM match an asymmetric fragment of **2** comprising a hexayne with only one methyl carboxylate group

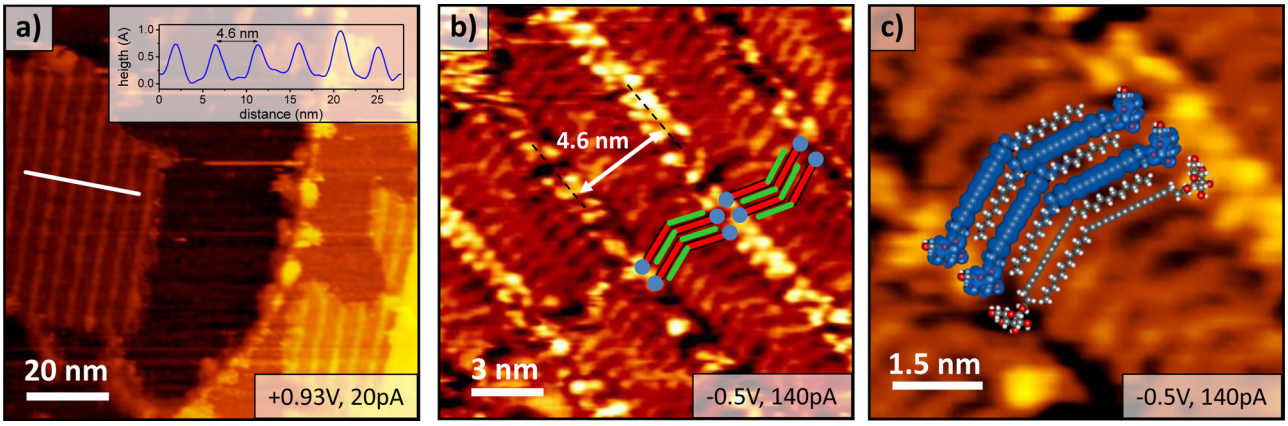

Fig. 4. STM images of a Au(1 1 1) surface after deposition of the glycosylated hexayne **1**. (a) The intact molecule self-assembles into islands with bright stripes. (b) A close-up scan provides submolecular resolution and shows ribbons with a width of 4.6 nm with interlocked molecules. (c) DFT computations of the glycosylated hexayne **1** is in agreement with observation that high intensity regions correspond to the carbohydrate and hexayne moieities.

(blue). Consequently, the fragments appear to be the result of a decarboxylation reaction in the ion beam.

The molecules in the islands are aligned in a head-to-head and tail-to-tail motif as depicted in Fig. 5b and c. This suggests an amphiphilic structural motif similar to the glycosylated hexayne **1**, stabilized by dipolar interactions of the head groups and dispersive interactions of π-conjugated hexayne segments. Since the polar methyl carboxylate head group of **2** has a significantly smaller footprint than the carbohydrate head group of **1**, a double ribbon growth is possible for **2** and apparently favored over an alternating interlocked mode as observed for **1**. A closer inspection of the island topography shows that the shape of the molecules features a kink (see Fig. 5 b,c) that, by analogy to the kink at the hexayne-alkyl connection in the case of **1**, can be assigned to the propyl spacer and the hexayne chain. Moreover, in the island with additional rows of high intensity lobes (Fig. 5c), the molecules feature a second kink next to an intense protrusion, suggesting that the linear *sp*-carbon chain of the hexayne segment has, in some way, been interrupted.

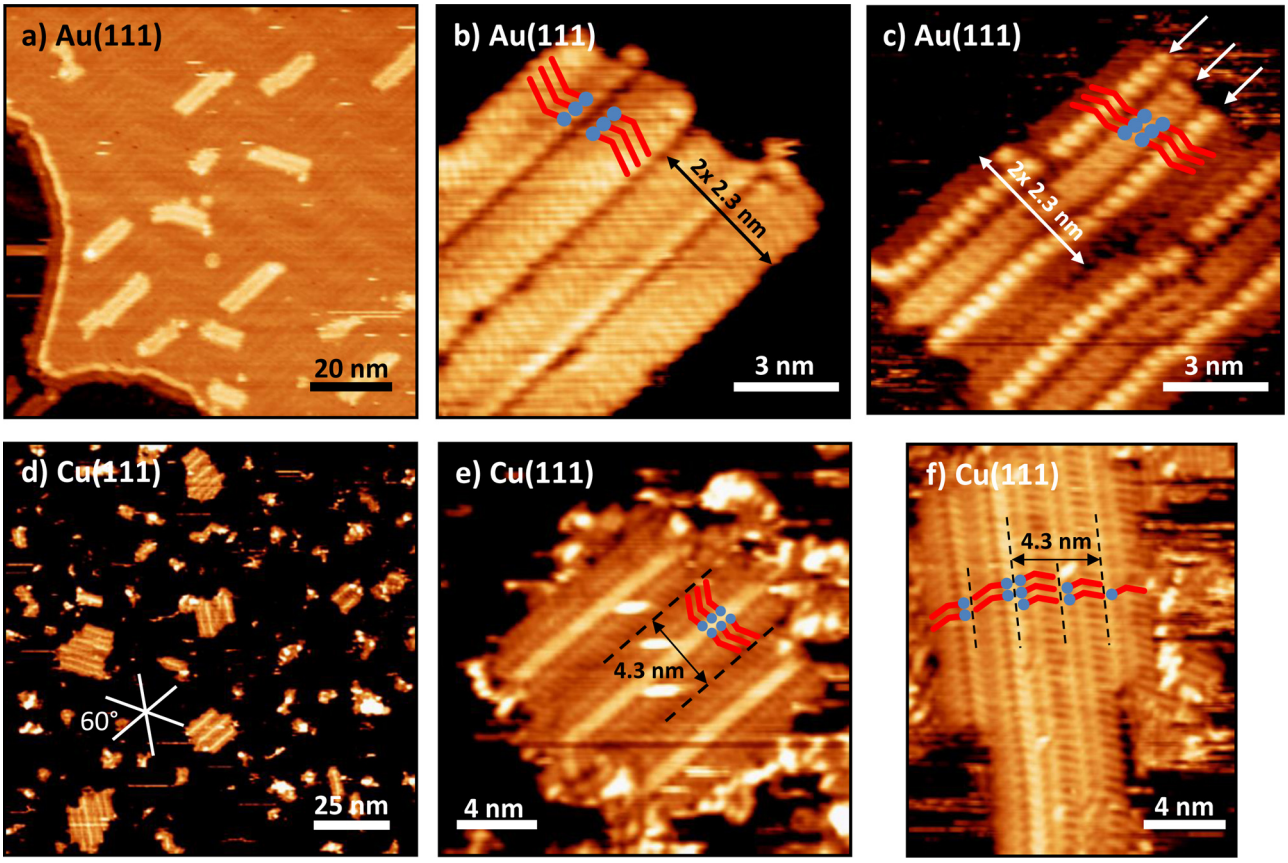

Fig. 5. STM images of the hexayne diester **2** on Au(1 1 1) and Cu(1 1 1) at low temperatures. (a) Ribbon-like island growth on Au(1 1 1) along the elbow site of the gold surface reconstruction. (b and c) Sub-molecular resolution of the islands show two different contrasts within the ribbons, that are 2.3 nm wide and appear in pairs of 4.6 nm width. Molecules are ordered in a head-to-head and tail-to-tail motif with a head (blue) and tail (red). (d) Islands on Cu(1 1 1) are aligned along the three directions of the hexagonal surface symmetry. (e and f) Close-up scans of the islands exhibit mixed ordering of the a molecule in a head-to-head and head-to-tail arrangement with a similar pair width of 4.3 nm.

Hence, the islands on Au(1 1 1) are clearly formed from fragments of the hexayne diester **2**. Their shape and size appears to be uniform, however, which seems to contradict the presence of various fragments in the corresponding mass spectrum. Streaks frequently observed in the STM images indicate that, despite the low temperature imaging, mobile molecules are present at the surface. In order to be able to immobilize these molecules as well, the Cu(1 1 1) surface was chosen for further investigations, since it interacts stronger with adsorbates and may inhibit molecular diffusion more efficiently. Both the intact hexayne diester **2** itself as well as very small fragments are excluded from the deposition this time by mass selection of the m/z range of 250–300 Th.

Since STM imaging on the Cu(1 1 1) surface at room temperature did not show any immobilized structures, it was carried out at a temperature of 40 K. At this temperature STM images of the surface showed similar ribbon-like islands with bright stripes as observed on Au(1 1 1), aligned along three directions at an angle of 60°, in accordance with the surface symmetry (Fig. 5d–f). In addition, disordered agglomerations surrounding the islands are also observed. The islands on Cu(1 1 1) are, again, constituted from ribbons composed of asymmetrical building blocks comprising a single kink. The width of a double ribbon on Cu(1 1 1) of 4.3 nm is almost equal to the width observed on the gold surface (4.6 nm). In addition to the head-to-head/tail-to-tail configuration of the ribbons on Au(1 1 1), a head-to-tail arrangement is sometimes observed on Cu(1 1 1), which means that paired as well as unpaired ribbons are present. This becomes obvious since the dominant bright stripes along the ribbons are only produced by the head-to-head configuration, while the coupling line between two ribbons is less pronounced in the head-to-tail configuration. The shape identified for the single molecule matches the shape found for the Au(1 1 1) islands closely, suggesting that the same species are observed on Au(1 1 1) and Cu(1 1 1). The disordered surroundings of the ordered islands, however, indicates that only certain hexayne diester fragments can form ribbons on Cu(1 1 1), while the variety of other fragments is frozen out into unordered patches.

5. Summary and conclusion

In summary, the successful deposition of sensitive oligoyne derivatives and their fragments with $n = 6$ conjugated triple bonds was demonstrated by means of ES-IBD. The soft ionization by ESI generates intact molecular ions or fragments with a still intact hexayne segment.

The molecules or fragments are detected on the surface by high resolution STM imaging, which allowed us to identify the molecular shape and the structure of agglomerations. The asymmetric glycosylated hexayne **1** has turned out to be more stable under the ionization and deposition conditions, and arranges into an interlocked ribbon structure of intact molecules. By contrast, the symmetric hexayne diester **2** largely underwent fragmentation, supposedly, because the chosen methyl carboxylate head groups can be eliminated following ionization-induced decarboxylation pathways. Nevertheless, certain fragments of **2** were observed to give rise to ordered surface structures, in which they were arranged into double ribbons by parallel alignment of the still intact hexayne segments.

Hence, the choice of substituents can be used to influence the ionization yield, the creation of fragments, as well as the molecular arrangement on the surface. We find that the substituents do not need to provide specific binding sites. Instead, the amphiphilic character of the hexayne molecules is a straightforward structural motif that is sufficient to achieve long range order and promotes anisotropic growth.

With reactive, carbon-rich molecular precursors like the two hexayne **1** and **2** investigated here, the rational fabrication of novel types of carbon materials on surfaces, for instance graphene nanoribbons (GNR), can be envisioned [44–47]. Such a fabrication route may intrinsically result in GNRs with well-defined edges and chemical functionalities, which would allow to adjust their electronic properties [48–52]. However, since the molecules are very mobile on the surface, thermal activation does not seem to be a good choice for initiating a carbonization reaction at low coverage [53,54]. Instead, UV-light or electron irradiation [33,34], or using catalytic surfaces [55,56] appear to be more feasible routes. Indeed such mild activation conditions are available when using reactive precursors like OY derivatives, for which we have shown the deposition and assembly here. While metal surfaces are required for STM characterization of the deposits, the use of an insulating surface geared toward materials preparation for device fabrication is well within the scope of the electrospray deposition technique [23,38].

Acknowledgment

F.R. is grateful to the Canada Research Chairs program for partial salary support and acknowledges the Alexander von Humboldt Foundation for a F.W. Bessel Award. H.F., S.S., and T.N.H. gratefully acknowledge funding from the European Research Council (ERC Grant 239831, 'OrgElNanoCarbMater') and ETH Zurich (Projekt ETH-05 08-2). S.R. and G.R. are grateful for support from Agilent Technologies.

References

[1] J.B. Fenn, M. Mann, C.K. Meng, S.F. Wong, C.M. Whitehouse, Science 246 (1989) 64–71.
[2] M. Karas, D. Bachmann, U. Bahr, F. Hillenkamp, Int. J. Mass Spectrom. Ion Process. 78 (1987) 53–68.
[3] E. de Hoffmann, V. Stroobant, Mass Spectrometry Principles and Applications, John Wiley & Sons Ltd., Chichester, West Sussex, England, 2007.
[4] V. Franchetti, B.H. Solka, W.E. Baitinger, J.W. Amy, R.G. Cooks, Int. J. Mass Spectrom. Ion Process. 23 (1977) 29–35.
[5] S. Rauschenbach, F.L. Stadler, E. Lunedei, N. Malinowski, S. Koltsov, G. Costantini, K. Kern, Small 2 (2006) 540–547.
[6] O. Hadjar, P. Wang, J.H. Futrell, Y. Dessiaterik, Z. Zhu, J.P. Cowin, M.J. Iedema, J. Laskin, Anal. Chem. 79 (2007) 6566–6574.
[7] C. Hamann, R. Woltmann, I.-P. Hong, N. Hauptmann, S. Karan, R. Berndt, Rev. Sci. Instrum. 82 (2011) 033903.
[8] B. Gologan, J.R. Green, J. Alvarez, J. Laskin, R.G. Cooks, Phys. Chem. Chem. Phys. 7 (2005) 1490–1500.
[9] G.E. Johnson, Q. Hu, J. Laskin, Annu. Rev. Anal. Chem. 4 (2011) 83–104.
[10] G. Verbeck, W. Hoffmann, B. Walton, Analyst 137 (2012) 4393–4407.
[11] E.T. Ada, O. Kornienko, L. Hanley, J. Phys. Chem. B 102 (1998) 3959–3966.
[12] N. Wade, C. Evans, S.-C. Jo, R.G. Cooks, J. Mass Spectrom. 37 (2002) 591–602.
[13] P. Wang, O. Hadjar, P.L. Gassman, J. Laskin, Phys. Chem. Chem. Phys. 10 (2008) 1512–1522.
[14] F. Mazzei, G. Favero, M. Frasconi, A. Tata, F. Pepi, Chem. – Eur. J. 15 (2009) 7359–7367.
[15] G.E. Johnson, J. Laskin, Chem. – Eur. J. 16 (2010) 14433–14438.
[16] S. Nagaoka, K. Ikemoto, K. Horiuchi, A. Nakajima, J. Am. Chem. Soc. 133 (2011) 18719–18727.
[17] N. Thontasen, G. Levita, N. Malinowski, Z. Deng, S. Rauschenbach, K. Kern, J. Phys. Chem. C 114 (2010) 17768–17772.
[18] Z. Deng, N. Thontasen, N. Malinowski, G. Rinke, L. Harnau, S. Rauschenbach, K. Kern, Nano Lett. 12 (2012) 2452–2458.
[19] S. Kahle, Z. Deng, N. Malinowski, C. Tonnoir, A. Forment-Aliaga, N. Thontasen, G. Rinke, D. Le, V. Turkowski, T.S. Rahman, S. Rauschenbach, M. Ternes, K. Kern, Nano Lett. 12 (2012) 518–521.
[20] N. Hauptmann, C. Hamann, H. Tang, R. Berndt, J. Phys. Chem. C 117 (2013) 9734–9738.
[21] C.S. Kley, C. Dette, G. Rinke, C.E. Patrick, J. Cechal, S.J. Jung, M. Baur, M. Dürr, S. Rauschenbach, F. Giustino, S. Stepanow, K. Kern, Nano Lett. 14 (2014) 563–569.
[22] H.J. Räder, A. Rouhanipour, A.M. Talarico, V. Palermo, P. Samori, K. Müllen, Nat. Mater. 5 (2006) 276–280, 31.
[23] S. Rauschenbach, G. Rinke, N. Malinowski, R.T. Weitz, R. Dinnebier, N. Thontasen, Z. Deng, T. Lutz, P.M. de Almeida Rollo, G. Costantini, L. Harnau, K. Kern, Adv. Mater. 24 (2012) 2761–2767.
[24] L. Lafferentz, V. Eberhardt, C. Dri, C. Africh, G. Comelli, F. Esch, S. Hecht, L. Grill, Nat. Chem. 4 (2012) 215–220.
[25] T.N. Hoheisel, S. Schrettl, R. Szilluweit, H. Frauenrath, Angew. Chem. Int. Ed. 49 (2010) 6496–6515.

[26] E.T. Chernick, R.R. Tykwinski, J. Phys. Org. Chem. 26 (2013) 742–749.
[27] J.-F. Morin, Synlett 24 (16) (2013) 2032–2044.
[28] S. Schrettl, C. Stefaniu, C. Schwieger, G. Pasche, E. Oveisi, Y. Fontana, A. Fontcuberta i Morral, J. Reguera, R. Petraglia, C. Corminboeuf, G. Brezesinski, H. Frauenrath, Nat. Chem. 6 (2014) 468–476.
[29] R. Szilluweit, T.N. Hoheisel, M. Fritzsche, B. Ketterer, A. Fontcuberta i Morral, D. Demurtas, V. Laporte, R. Verel, S. Bolisetty, R. Mezzenga, Nano Lett. 12 (2012) 2573–2578.
[30] S. Szafert, J.A. Gladysz, Chem. Rev. 106 (2006) PR1–PR33.
[31] R.R. Tykwinski, W.A. Chalifoux, S. Eisler, A. Lucotti, M. Tommasini, D. Fazzi, M. Del Zoppo, G. Zerbi, Pure Appl. Chem. 82 (2010) 891–904.
[32] W.A. Chalifoux, R.R. Tykwinski, Nat. Chem. 2 (2010) 967–971.
[33] A. Miura, S. De Feyter, M.M.S. Abdel-Mottaleb, A. Gesquiere, P.C.M. Grim, G. Moessner, M. Sieffert, M. Klapper, K. Müllen, F.C. De Schryver, Langmuir 19 (2003) 6474–6482.
[34] T. Takami, H. Ozaki, M. Kasuga, T. Tsuchiya, A. Ogawa, Y. Mazaki, D. Fukushi, M. Uda, M. Aono, Angew. Chem. Int. Ed. 36 (1997) 2755–2757.
[35] A. Deshpande, C.-H. Sham, J.M.P. Alaboson, J.M. Mullin, G.C. Schatz, M.C. Hersam, J. Am. Chem. Soc. 134 (2012) 16759–16764.
[36] T.N. Hoheisel, H. Frauenrath, Org. Lett. 10 (2008) 4525–4528.
[37] M. Pauly, M. Sroka, J. Reiss, G. Rinke, A. Albarghash, R. Vogelgesang, H. Hahne, B. Kuster, J. Sesterhenn, K. Kern, S. Rauschenbach, Analyst 139 (2014) 1856–1867.
[38] J. Laskin, P. Wang, O. Hadjar, Phys. Chem. Chem. Phys. 10 (2008) 1079–1090.
[39] S. Rauschenbach, R. Vogelgesang, N. Malinowski, J.W. Gerlach, M. Benyoucef, G. Costantini, Z. Deng, N. Thontasen, K. Kern, ACS Nano 3 (2009) 2901–2910.
[40] F. Neese, WIREs Comput. Mol. Sci. 2 (2012) 73–78.
[41] R.G. Cooks, A.L. Rockwood, Rapid Commun. Mass Spectrom. 5 (1991) 93.
[42] M.M. Blake, S.U. Nanayakkara, S.A. Claridge, L.C. Fernandez-Torres, E.C.H. Sykes, P.S. Weiss, J. Phys. Chem. A 113 (2009) 13167–13172.
[43] J.V. Barth, H. Brune, G. Ertl, R.J. Behm, Phys. Rev. B 42 (1990) 9307–9318.
[44] J. Cai, P. Ruffieux, R. Jaafar, M. Bieri, T. Braun, S. Blankenburg, M. Muoth, A.P. Seitsonen, M. Saleh, X. Feng, K. Müllen, R. Fasel, Nature 466 (2010) 470–473.
[45] K. Amsharov, N. Abdurakhmanova, S. Stepanow, S. Rauschenbach, M. Jansen, K. Kern, Angew. Chem. 122 (2010) 9582–9586.
[46] L. Chen, Y. Hernandez, X. Feng, K. Müllen, Angew. Chem. Int. Ed. 51 (2012) 7640–7654.
[47] D.G. de Oteyza, P. Gorman, Y.-C. Chen, S. Wickenburg, A. Riss, D.J. Mowbray, G. Etkin, Z. Pedramrazi, H.-Z. Tsai, A. Rubio, M.F. Crommie, F.R. Fischer, Science 340 (2013) 1434–1437.
[48] M. Fujita, K. Wakabayashi, K. Nakada, K. Kusakabe, J. Phys. Soc. Jpn. 65 (1996) 1920–1923.
[49] K. Nakada, M. Fujita, G. Dresselhaus, M.S. Dresselhaus, Phys. Rev. B 54 (1996) 17954–17961.
[50] K. Wakabayashi, M. Fujita, H. Ajiki, M. Sigrist, Phys. Rev. B 59 (1999) 8271–8282.
[51] V. Barone, O. Hod, G.E. Scuseria, Nano Lett. 6 (2006) 2748–2754.
[52] Y.-W. Son, M.L. Cohen, S.G. Louie, Nature 444 (2006) 347–349.
[53] L. Grill, M. Dyer, L. Lafferentz, M. Persson, M.V. Peters, S. Hecht, Nat. Nanotech. 2 (2007) 687–691.
[54] R. Gutzler, L. Cardenas, J. Lipton-Duffin, M. El Garah, L.E. Dinca, C.E. Szakacs, C. Fu, M. Gallagher, M. Vondráĉek, M. Rybachuk, D.F. Perepichka, F. Rosei, Nanoscale 6 (2014) 2660–2668.
[55] F. Monnier, M. Taillefer, Angew. Chem. Int. Ed. 47 (2008) 3096–3099.
[56] J.A. Lipton-Duffin, J.A. Miwa, M. Kondratenko, F. Cicoira, B.G. Sumpter, V. Meunier, D.F. Perepichka, F. Rosei, Proc. Natl. Acad. Sci. 107 (2010) 11200–11204.